

Title:

Staging Liver Fibrosis by Fibroblast Activation Protein Inhibitor Positron Emission Tomography  
in a Human-sized Swine Model

Running title:

FAPI PET for staging Liver Fibrosis

Authors:

1. Ali Pirasteh, MD <sup>1</sup>
2. Sarvesh Periyasamy, MS <sup>2</sup>
3. Jennifer Jean Meudt, MS <sup>3</sup>
4. Yongjun Liu, MD, PhD <sup>4</sup>
5. Laura M. Lee, MA, DVM, DACVP <sup>5</sup>
6. Kyle M. Schachtschneider, PhD <sup>6,7</sup>
7. Lawrence B. Schook, PhD <sup>8,9</sup>
8. Ron C. Gaba, MD, MS <sup>9</sup>
9. Lu Mao, PhD <sup>10</sup>
10. Adnan Said, MD, MS <sup>11,12</sup>
11. Alan Blair McMillan, PhD <sup>1</sup>
12. Paul F Laeseke, MD PhD <sup>2</sup>
13. Dhanansayan Shanmuganayagam, PhD <sup>3,13,14</sup>

Affiliations:

<sup>1</sup> Radiology and Medical Physics, University of Wisconsin-Madison, USA

<sup>2</sup> Radiology and Biomedical Engineering, University of Wisconsin-Madison, USA

<sup>3</sup> Animal and Dairy Sciences, University of Wisconsin-Madison, USA

<sup>4</sup> Pathology and Laboratory Medicine, University of Wisconsin-Madison, USA

<sup>5</sup> Research Animal Resources and Compliance, University of Wisconsin-Madison, USA

<sup>6</sup> Radiology and Biochemistry & Molecular Genetics, University of Illinois at Chicago, USA

<sup>7</sup> National Center for Supercomputing Applications, University of Illinois at Urbana-Champaign,  
USA

<sup>8</sup> Animal Sciences, University of Illinois at Chicago, USA

<sup>9</sup> Radiology/Interventional Radiology, University of Illinois at Chicago, USA

<sup>10</sup> Biostatistics and Medical Informatics, University of Wisconsin-Madison, USA

<sup>11</sup> Medicine, Gastroenterology and Hepatology, University of Wisconsin-Madison, USA

<sup>12</sup> William S. Middleton VA Medical Center, Madison, WI, USA

<sup>13</sup> Surgery, University of Wisconsin-Madison, USA

<sup>14</sup> Center for Biomedical Swine Research and Innovation, University of Wisconsin-Madison, USA

Corresponding author (NOT in training):

Ali Pirasteh, MD

1111 Highland Ave., WIMR 2423

Madison, WI 53705

Phone: 608-265-6044; fax: 608-265-7390; email: pirasteh@wisc.edu

Word Count

4972

Financial support Statement:

Sarvesh Periyasamy: supported by National Cancer Institute (Award Number F30CA250408) and National Institute of General Medical Sciences (Award Number T32GM140935). This work was supported in-part by the Biomedical & Genomic Research Group Discretionary Fund (University of Wisconsin-Madison).

## **ABSTRACT**

*Rationale.* Current methods of staging liver fibrosis have notable limitations. We investigated the utility of positron emission tomography (PET) in staging liver fibrosis by correlating liver uptake of  $^{68}\text{Ga}$ -labeled fibroblast activation protein inhibitor (FAPI) with histology in a human-sized swine model.

*Methods.* Five pigs underwent baseline FAPI PET/MRI and liver biopsy, followed by liver parenchymal embolization, 8 weeks of oral alcohol intake, endpoint FAPI PET/MRI, and necropsy. Regions of interest (ROIs) were drawn on baseline and endpoint PET images and mean standardized uptake values (SUVs) were recorded. At endpoint, liver sections corresponding to ROIs were identified and cut out. Histologic evaluation of fibrosis was performed using a modified METAVIR score for swine liver and quantitatively using collagen proportionate area (CPA). Box-and-whisker plot and linear regression were used to correlate SUV with METAVIR score and CPA, respectively.

*Results.* Liver FAPI uptake strongly correlated with CPA (Pearson correlation coefficient,  $r=0.89$ ,  $P<0.001$ ). FAPI uptake was significantly and progressively higher across F2 and F3/F4 fibrosis stages, respective median SUVs [interquartile range, IQR] of 2.9 [2.7 – 3.8] and 7.6 [6.7 – 10.2] ( $P<0.001$ ). There was no significant difference between FAPI uptake of baseline liver and endpoint liver sections staged as F0/F1, respective median SUVs [IQR] of 1.7 [1.3 – 2.0] and 1.7 [1.5 – 1.8] ( $P = 0.338$ ).

*Conclusion.* The strong correlation between liver FAPI uptake and the histologic stage of liver fibrosis suggests FAPI PET can play an impactful role in noninvasive staging of liver fibrosis, pending validation in patients.

*Keywords.*

Fibroblast activation protein inhibitor

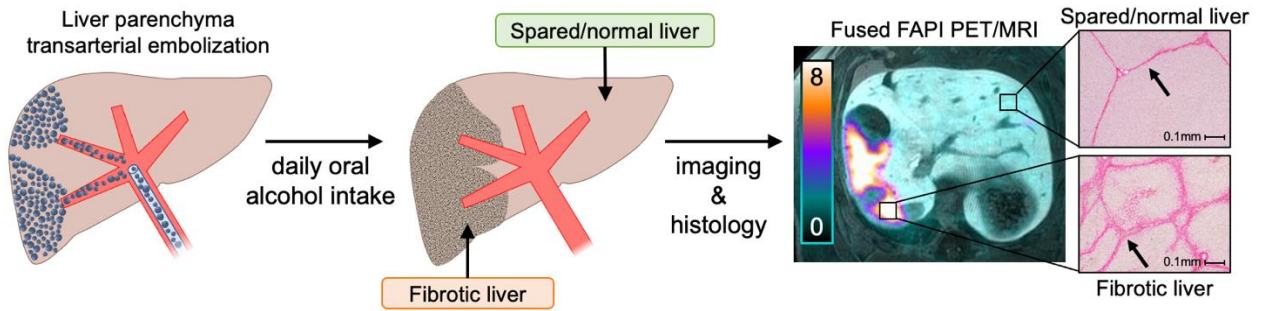
Liver Fibrosis

Positron emission tomography

Magnetic resonance imaging

Swine

*Graphical Abstract.*



## INTRODUCTION

Liver fibrosis is the consequence of chronic liver injury of any etiology and affects >120 million people worldwide.(1,2) End-stage liver fibrosis (i.e., cirrhosis) is the global leading cause of liver-disease-related deaths and the most important risk factor for developing liver cancer.(1) Fibrosis is the only histologic feature that predicts long-term outcomes, and serial assessments of fibrosis are of key prognostic importance in patient outcomes and assessing treatment response.(3) Although transplant remains the only available cure for decompensated end-stage liver fibrosis, earlier stages of liver injury and fibrosis are treatable and reversible.(4,5)

Current methods of assessing liver fibrosis have notable limitations. Laboratory markers are unreliable,(6,7) and liver biopsy (the current gold standard) carries morbidity/mortality risks and is prone to undersampling and sampling/interpretation variability.(8-13) Magnetic resonance elastography (MRE) is the best validated noninvasive tool and estimates liver stiffness as a surrogate for the histologic fibrosis stage.(14-18) MRE has lower sensitivity for detection of lower stages of fibrosis, can be nondiagnostic due to liver iron overload or operator error, and cannot differentiate fibrosis from concurrent liver inflammation as both processes increase liver stiffness.(18-20) Hence there remains a clear unmet need for a noninvasive, quantitative, and accurate tool for staging liver fibrosis.

Fibroblast activation protein (FAP) is a cell surface peptidase expressed in disease processes with matrix remodeling, such as by the fibrogenic liver stellate cells.(21,22) Radiolabeled FAP inhibitors (FAPI) have been utilized with positron emission tomography (PET) to target FAP in vivo as an imaging tool.(23,24) Advantages of PET include quantitative radiotracer uptake evaluation by standardized uptake value (SUV) and relatively operator-independent, simple whole-liver imaging. Hence, the goal of this study was to prospectively

investigate the correlation between liver FAPI uptake on PET and the gold standard histologic stage of liver fibrosis in a human-sized swine model of alcohol-induced liver fibrosis.

## **MATERIALS AND METHODS**

This study was conducted under protocols approved by local Institutional Animal Care and Use Committee in accordance with published National Institutes of Health and U.S. Department of Agriculture guidelines. Figure 1 summarizes the study design. The utilized swine model has been demonstrated to successfully induce liver fibrosis(25,26) and is detailed in the Supplemental Data section. Five human-sized, age-matched male Wisconsin Miniature Swine™ underwent same-day PET/MRI and core-needle liver biopsy to establish baseline histologic and imaging characteristics of the liver. Increasing volumes of ethanol were then added to their daily diets over a 7-day period, followed by transarterial liver embolization with an emulsion of ethanol and ethiodized oil. Animals continued oral alcohol intake for 8 more weeks, after which they underwent endpoint PET/MRI and necropsy.

*Imaging.* Images were acquired under general anesthesia in the supine position on a whole-body PET/MRI scanner (Signa PET/MR, GE Healthcare, Chicago, IL, USA). Continuous dynamic PET data of the liver were acquired for 92 minutes; <sup>68</sup>Ga-FAPI-46 was administered intravenously 1 minute after the initiation of data acquisitions: average (range) dose of 4.3 (3.5 – 4.6) MBq/kg body weight. Attenuation-corrected dynamic PET images were reconstructed with 15 seconds/frame for the first 5 minutes and 3 minutes/frame for the rest of the acquisition. An additional static image was generated at 60 minutes post radiotracer injection (using PET data at 60-69 minutes). Images were reviewed and analyzed by a dual board-certified nuclear medicine physician/radiologist with fellowship training in abdominal imaging and nuclear medicine, using

MIM software (version 7.1.2). Image analysis was performed prior to histologic tissue assessment to minimize bias.

*Baseline Image Analysis.* Circular regions of interest (ROIs) were placed on the liver parenchyma on MRI, avoiding major vessels, one in the right lobe and one in the left lobe, with a minimum diameter of 1.5 cm. Each ROI was propagated across one slice cranially and one slice caudally, yielding a cylindrical ROI with a minimum volume of 4 cm<sup>3</sup>. To minimize bias, ROIs were directly propagated by the software into both dynamic and static PET images.  $SUV_{\text{mean}}$  (herein SUV) for each ROI was recorded, yielding 10 data points at baseline (2 per animal).

*Endpoint Image Analysis.* Due to the heterogeneous nature of the fibrosis achieved by this model (dictated by preferential liver arterial flow carrying different volumes of embolic emulsion to different liver regions), for each animal four ROIs were placed on the static PET images as follows: to achieve adequate assessment across the uptake spectrum, two ROIs were placed on most avid areas and two on relatively less avid areas. Second, ROIs were placed in areas that could be localized on harvested livers using anatomic landmarks (e.g., gallbladder fossa, major vessels, etc.). This approach yielded 20 data points at endpoint (4 per animal).

*Tissue procurement and histology.* Baseline core samples were obtained from each liver lobe. Livers were harvested at endpoint, and lobar surfaces were marked with ink to preserve the landmarks needed for imaging-histology co-localization. Livers were sectioned using a “bread-loafing” technique in the axial plane to resemble the slices on PET/MRI, and all slices were fixed

in formalin. Using anatomic landmarks, liver areas corresponding to the ROIs on endpoint images were identified, and wedge sections from these regions were cut out.

All tissue samples were processed with Masson's Trichrome stain, Picrosirius red stain, and anti-FAP immunohistochemistry. Histologic review and analysis were carried out by a board-certified fellowship-trained hepatobiliary pathologist, blinded to imaging results and the timepoints of tissue procurement. Two histologic standards were used as reference: METAVIR fibrosis score(27,28) and collagen proportionate area (CPA).(29-35) The METAVIR score is an ordinal five-point scale (F0 to F4), where in humans F0 is absence of fibrosis and F4 is end-stage fibrosis/cirrhosis. Given that normal swine liver has thin, organized bands of fibrosis, for the purposes of this study, F0 and F1 were grouped into one category (F0/F1) and assigned to normal swine liver (Figure 2). CPA is the proportion of collagen deposition area relative to the total tissue area (reported in %) on Picrosirius red-stained slides. CPA analysis was performed only for endpoint wedge sections and not for baseline tissues, due to the relatively small amount of tissue procured through core needle biopsy at baseline.

*Statistical analysis.* Liver FAPI uptake time-activity curves were generated by plotting the pooled ROI SUVs against time for different stages of fibrosis. Box-and-whisker plots were generated to compare liver FAPI uptake and CPA across different histologic stages of liver fibrosis, using Kruskal-Wallis rank sum test. Linear regression was used to correlate liver FAPI with CPA, using the Pearson correlation coefficient. To account for the correlation among repeated measurements and their non-monotone change over time, a linear mixed effects model was used with pig- and ROI-specific random effects and piecewise linear time trend. Time-activity curves were compared using an F-test on longitudinal measurements assuming normally distributed



errors.  $P < 0.05$  was considered statistically significant. A post-hoc power analysis for testing F2 versus F0/F1, and F3/F4 versus F0/F1 stages under the current sample size was performed.

## RESULTS

All animals completed the study procedures. Baseline PET imaging of animal #2 was terminated at 69 minutes post injection due to need for removal of the animal from the scanner to re-establish airway and ensure animal safety. For animal #3, PET data at 37-42 min were discarded due to a shift in animal's position inside the scanner during that time period, but imaging was completed successfully. Time-activity curves demonstrated incrementally higher delayed FAPI uptake of stage F2 and F3/F4 sections ( $P < 0.001$ , Figure 3). Uptake was stabilized at 60 minutes, the timepoint at which the static images were generated for the purposes of quantitative analysis and imaging-histologic correlation.

Figure 4 is an example of imaging-histology correlation in the same animal at baseline and at endpoint, where the embolized region of the liver demonstrated fibrosis with avid FAPI uptake. Table 1 summarizes the FAPI uptake and the corresponding METAVIR score and CPA for all liver sections. Baseline liver samples were all normal (stage F0/F1). At endpoint, of the total 20 liver sections, nine staged as F0/F1, three as F2, one as F3, and seven as F4. Given only one specimen was staged as F3, it was grouped with the F4 specimens (i.e., group F3/F4) to provide for a meaningful quantitative analysis.

There was a strong linear correlation between liver FAPI uptake and histologic CPA ( $r = 0.89$ ,  $P < 0.001$ , Figure 5A). There was no significant difference between the uptake of baseline liver and endpoint liver sections staged as F0/F1, respective median SUVs [interquartile range, IQR] of 1.7 [1.3 – 2.0] and 1.7 [1.5 – 1.8] ( $P = 0.338$ ). Conversely, FAPI uptake was significantly higher across F2 and F3/F4 stages and directly correlated with the histologic fibrosis stage,

respective median SUVs [IQR] of 2.9 [2.7 – 3.8] and 7.6 [6.7 – 10.2] ( $P < 0.001$ , Figure 5B). There was also a significant increase of CPA across fibrosis stages, median CPA [IQR] of 14% [13% – 16%] for F0/F1, 33% [31% – 36%] for F2, and 49% [47% – 61%] for F3/F4 (all  $P < 0.001$ , Figure 5C). The post-hoc power of testing F2 versus F0/F1, and F3/F4 versus F0/F1 under the current sample size was calculated as respectively 44% and 99.99%.

## DISCUSSION

We demonstrated that liver FAPI uptake strongly correlates with two accepted histologic metrics of liver fibrosis across the observed fibrosis stages in a human-sized swine model. Other molecular imaging agents have also been investigated for this purpose. Increased liver uptake of  $^{18}\text{F}$ -alfatide in more advanced stages of fibrosis in a mouse model has been reported.(36) However, normal liver uptake of  $^{18}\text{F}$ -alfatide appears to be substantial enough to render this agent suboptimal for discerning lower stages of fibrosis.(36,37) A study of  $^{11}\text{C}$ -aminoglycerol PET in a rat model demonstrated an inverse correlation between liver radiotracer uptake and fibrosis stage. Key limitations of this approach include very short radiotracer half-life and overlap of uptake intensity between fibrosis stages.(38) Last,  $^{18}\text{F}$ -fluorodeoxyglucose (FDG) PET plays only a limited role in evaluation of liver fibrosis, mainly due to altered liver glucose metabolism in the setting of chronic liver disease. (39)

FAPI PET can offer several key potential advantages for evaluation of liver fibrosis. In our human-sized swine model, FAPI differentiated between various stages of disease. Furthermore, considering minimal uptake in normal human liver,(40,41) FAPI may detect early changes of fibrosis, which would be advantageous over elastography. Additional advantages of FAPI PET over elastography would be whole-liver evaluation, minimal opportunity for operator error, and robustness against factors that contribute to or confound liver stiffness measurement, most notably

concurrent liver inflammation.(16) Although a more novel 3D MRE technique has demonstrated potential to address this limitation,(42) this concept has not been validated in clinical practice. However, considering the ability of MRI in accurate assessment of several key aspects of diffuse liver disease, such as fat, iron, and stiffness,(43,44) it is likely that combined FAPI PET and MRI/MRE may provide complementary information to paint a more complete picture of the state of liver disease. Potential disadvantages of FAPI PET include radiation exposure and radiotracer availability. However, human dosimetry of FAPI has demonstrated a whole-body exposure that is similar to that of FDG.(41,45) There remain challenges and unknowns that should be addressed as part of further validation of FAPI PET's utility in assessment of liver fibrosis. While FAPI uptake directly correlated with the stage of fibrosis in the presented model, this correlation was observed in the setting of active fibrosis where the animals continued alcohol intake on a daily basis. Whether this observation is reproducible in other chronic disease processes, such as in viral hepatitis and non-alcoholic steatohepatitis, is of significant scientific and clinical relevance and requires further validation.

This study has some limitations. While the sample size was small, post-hoc power analysis demonstrated its adequacy, which is also at par with a previous report.(46) Furthermore, this model generated patchy/geographic areas of fibrotic and normal liver, which is different than the pattern of disease in humans. However, this feature allowed for an internal negative control. Another limitation of a swine model is presence of thin fibrotic bands in normal liver, explaining normal liver's FAPI uptake. Hence, FAPI PET's potential in differentiating between F0 and F1 stages of disease would have to be investigated in human subjects. Our data yielded only one specimen with F3 liver fibrosis; hence, we are unable to evaluate FAPI PET's ability to discern between F3 and F4 stages. We must note that while worth investigating, the significance of this limitation is

unknown, as often in clinical practice or in the research setting, F0 and F1 stages as well as F3 and F4 stages are grouped together for treatment and/or prognostic purposes. Last, despite the careful approach to achieve accurate and unbiased imaging-histology correlation through blinding and using only anatomic landmarks to obtain tissue samples that correspond to ROIs, sampling error/variability cannot be completely eliminated. This variability and limitation are not unique to this study and also present in the current clinical practice as well as in nearly all studies that have evaluated liver fibrosis. We anticipate that once FAPI PET for assessment of liver fibrosis is further investigated and potentially validated in humans, it will largely overcome the aforementioned limitations of the current techniques, and it will enhance our ability in understanding of disease progression and evolution among those with chronic liver disease.

## **CONCLUSION**

The strong correlation between liver FAPI uptake and the histologic stage of liver fibrosis suggests FAPI PET can play an impactful role in noninvasive staging of liver fibrosis, pending validation in patients. This technique can be utilized not only in the clinical setting, but also for clinical trials (e.g., drug development) or for validation of other novel techniques for assessment of diffuse liver disease.

## **KEY POINTS**

*Question.* Is there potential for FAPI PET in staging liver fibrosis?

*Pertinent Findings:* This animal study demonstrated a direct correlation between quantitative liver FAPI uptake on PET and both histologic measures of liver fibrosis, i.e., the ordinal METAVIR score and the quantitative collagen proportionate area.

*Implications for Patient Care:* Pending further validation in patients, FAPI PET is a promising tool for noninvasive liver fibrosis staging.

## **DISCLOSURES**

Ali Pirasteh: GE Healthcare (departmental research support); TheraCea, Sanofi Genzyme (consultant). Sarvesh Periyasamy: Johnson & Johnson, HEPTA Medical, Vector Surgical (consultant). Kyle Schachtschneider: Guerbet, Janssen Research & Development, NeoTherma Oncology, TriSalus Life Sciences (research support); Sus Clinicals, Inc. (consultant). Lawrence Schook: Guerbet, Janssen Research & Development, NeoTherma Oncology, TriSalus Life Sciences (research support); Sus Clinicals, Inc (Chief Scientific Officer). Ron Gaba: Guerbet, Janssen Research & Development, NeoTherma Oncology, TriSalus Life Sciences (research support); Sus Clinicals, Inc (consultant). Adnan Said: Intercept Pharmaceuticals, Exact sciences (research support). Paul Laeseke: Johnson & Johnson /Ethicon/NeuWave (consultant), HistoSonics (consultant, shareholder, research agreement), Elucent (consultant, shareholder), Siemens (research agreement), McGinley Orthopedic Innovations (shareholder). Dhanansayan Shanmuganayagam: Wisconsin Miniature Swine™ (Co-inventor). Jennifer Meudt, Yongjun Lui, Laura Lee, Lu Mao, Alan McMillan: None. No other potential conflicts of interest relevant to this article.

## REFERENCES

1. The global, regional, and national burden of cirrhosis by cause in 195 countries and territories, 1990-2017: a systematic analysis for the Global Burden of Disease Study 2017. *Lancet Gastroenterol Hepatol.* 2020;5:245-266.
2. Ge PS, Runyon BA. Treatment of patients with cirrhosis. *N Engl J Med.* 2016;375:767-777.
3. Angulo P, Kleiner DE, Dam-Larsen S, et al. Liver fibrosis, but no other histologic features, is associated with long-term outcomes of patients with nonalcoholic fatty liver disease. *Gastroenterology.* 2015;149:389-397.e310.
4. D'Ambrosio R, Aghemo A, Rumi MG, et al. A morphometric and immunohistochemical study to assess the benefit of a sustained virological response in hepatitis C virus patients with cirrhosis. *Hepatology.* 2012;56:532-543.
5. Marcellin P, Gane E, Buti M, et al. Regression of cirrhosis during treatment with tenofovir disoproxil fumarate for chronic hepatitis B: a 5-year open-label follow-up study. *Lancet.* 2013;381:468-475.
6. Alberti A, Noventa F, Benvegna L, Boccato S, Gatta A. Prevalence of liver disease in a population of asymptomatic persons with hepatitis C virus infection. *Ann Intern Med.* 2002;137:961-964.
7. Harris R, Harman DJ, Card TR, Aithal GP, Guha IN. Prevalence of clinically significant liver disease within the general population, as defined by non-invasive markers of liver fibrosis: a systematic review. *Lancet Gastroenterol Hepatol.* 2017;2:288-297.
8. Sumida Y. Limitations of liver biopsy and non-invasive diagnostic tests for the diagnosis of nonalcoholic fatty liver disease/nonalcoholic steatohepatitis. *World J Gastroenterol.* 2014;20:475.
9. Rousselet M-C, Michalak S, Dupré F, et al. Sources of variability in histological scoring of chronic viral hepatitis. *Hepatology.* 2005;41:257-264.
10. Goldin RD, Goldin JG, Burt AD, et al. Intra-observer variation in the histopathological assessment of chronic viral hepatitis. *J Hepatol.* 1996;25:649-654.
11. Maharaj B, Maharaj RJ, Leary WP, et al. Sampling variability and its influence on the diagnostic yield of percutaneous needle biopsy of the liver. *Lancet.* 1986;1:523-525.
12. Regev A, Berho M, Jeffers LJ, et al. Sampling error and intraobserver variation in liver biopsy in patients with chronic HCV infection. *Am J Gastroenterol.* 2002;97:2614-2618.
13. Bravo AA, Sheth SG, Chopra S. Liver biopsy. *N Engl J Med.* 2001;344:495-500.
14. Singh S, Venkatesh SK, Wang Z, et al. Diagnostic performance of magnetic resonance elastography in staging liver fibrosis: a systematic review and meta-analysis of individual participant data. *Clin Gastroenterol Hepatol.* 2015;13:440-451.e446.
15. Yin M, Woollard J, Wang X, et al. Quantitative assessment of hepatic fibrosis in an animal model with magnetic resonance elastography. *Magn Reson Med.* 2007;58:346-353.

16. Tang A, Cloutier G, Szeverenyi NM, Sirlin CB. Ultrasound elastography and MR elastography for assessing liver fibrosis: part 2, diagnostic performance, confounders, and future directions. *AJR Am J Roentgenol.* 2015;205:33-40.
17. Wang QB, Zhu H, Liu HL, Zhang B. Performance of magnetic resonance elastography and diffusion-weighted imaging for the staging of hepatic fibrosis: A meta-analysis. *Hepatology.* 2012;56:239-247.
18. Yin M, Glaser KJ, Talwalkar JA, Chen J, Manduca A, Ehman RL. Hepatic MR elastography: clinical performance in a series of 1377 consecutive examinations. *Radiology.* 2016;278:114-124.
19. Chen J, Talwalkar JA, Yin M, Glaser KJ, Sanderson SO, Ehman RL. Early detection of nonalcoholic steatohepatitis in patients with nonalcoholic fatty liver disease by using MR elastography. *Radiology.* 2011;259:749-756.
20. Salameh N, Larrat B, Abarca-Quinones J, et al. Early detection of steatohepatitis in fatty rat liver by using MR elastography. *Radiology.* 2009;253:90-97.
21. Levy MT, McCaughan GW, Abbott CA, et al. Fibroblast activation protein: a cell surface dipeptidyl peptidase and gelatinase expressed by stellate cells at the tissue remodelling interface in human cirrhosis. *Hepatology.* 1999;29:1768-1778.
22. Uitte De Willige S, Malfliet JJMC, Janssen HLA, Leebeek FWG, Rijken DC. Increased N-terminal cleavage of alpha-2-antiplasmin in patients with liver cirrhosis. *J Thromb Haemost.* 2013;11:2029-2036.
23. Shi X, Xing H, Yang X, et al. Fibroblast imaging of hepatic carcinoma with (68)Ga-FAPI-04 PET/CT: a pilot study in patients with suspected hepatic nodules. *Eur J Nucl Med Mol Imaging.* 2021;48:196-203.
24. Loktev A, Lindner T, Mier W, et al. A tumor-imaging method targeting cancer-associated fibroblasts. *J Nucl Med.* 2018;59:1423-1429.
25. Gaba RC, Mendoza-Elias N, Regan DP, et al. Characterization of an inducible alcoholic liver fibrosis model for hepatocellular carcinoma investigation in a transgenic porcine tumorigenic platform. *J Vasc Interv Radiol.* 2018;29:1194-1202.e1191.
26. Avritscher R, Wright KC, Javadi S, et al. Development of a large animal model of cirrhosis and portal hypertension using hepatic transarterial embolization: a study in swine. *J Vasc Interv Radiol.* 2011;22:1329-1334.
27. Intraobserver and interobserver variations in liver biopsy interpretation in patients with chronic hepatitis C. The French METAVIR Cooperative Study Group. *Hepatology.* 1994;20:15-20.
28. Bedossa P, Poinard T. An algorithm for the grading of activity in chronic hepatitis C. *Hepatology.* 1996;24:289-293.
29. Buzzetti E, Hall A, Ekstedt M, et al. Collagen proportionate area is an independent predictor of long-term outcome in patients with non-alcoholic fatty liver disease. *Aliment Pharmacol Ther.* 2019;49:1214-1222.

30. Tsochatzis E, Bruno S, Isgro G, et al. Collagen proportionate area is superior to other histological methods for sub-classifying cirrhosis and determining prognosis. *J Hepatol.* 2014;60:948-954.
31. Calvaruso V, Dhillon AP, Tsochatzis E, et al. Liver collagen proportionate area predicts decompensation in patients with recurrent hepatitis C virus cirrhosis after liver transplantation. *J Gastroenterol Hepatol.* 2012;27:1227-1232.
32. Manousou P, Burroughs AK, Tsochatzis E, et al. Digital image analysis of collagen assessment of progression of fibrosis in recurrent HCV after liver transplantation. *J Hepatol.* 2013;58:962-968.
33. Calvaruso V, Burroughs AK, Standish R, et al. Computer-assisted image analysis of liver collagen: relationship to Ishak scoring and hepatic venous pressure gradient. *Hepatology.* 2009;49:1236-1244.
34. Xie SB, Ma C, Lin CS, Zhang Y, Zhu JY, Ke WM. Collagen proportionate area of liver tissue determined by digital image analysis in patients with HBV-related decompensated cirrhosis. *Hepatobiliary Pancreat Dis Int.* 2011;10:497-501.
35. Isgro G, Calvaruso V, Andreana L, et al. The relationship between transient elastography and histological collagen proportionate area for assessing fibrosis in chronic viral hepatitis. *J Gastroenterol.* 2013;48:921-929.
36. Shao T, Chen Z, Belov V, et al. [(18)F]-Alfatide PET imaging of integrin  $\alpha v \beta 3$  for the non-invasive quantification of liver fibrosis. *J Hepatol.* 2020;73:161-169.
37. Wu J, Wang S, Zhang X, et al. 18F-Alfatide II PET/CT for identification of breast cancer: a preliminary clinical study. *J Nucl Med.* 2018;59:1809-1816.
38. Chen X, Zhang X, Du M, et al. In vivo preclinical PET/CT imaging of carbon-11-labeled aminoglycerol probe for the diagnosis of liver fibrosis. *Ann Nucl Med.* 2019;33:806-812.
39. Verloh N, Einspieler I, Utpatel K, et al. In vivo confirmation of altered hepatic glucose metabolism in patients with liver fibrosis/cirrhosis by (18)F-FDG PET/CT. *EJNMMI Res.* 2018;8:98.
40. Kratochwil C, Flechsig P, Lindner T, et al. 68Ga-FAPI PET/CT: tracer uptake in 28 different kinds of cancer. *J Nucl Med.* 2019;60:801-805.
41. Giesel FL, Kratochwil C, Lindner T, et al. 68Ga-FAPI PET/CT: biodistribution and preliminary dosimetry estimate of 2 DOTA-containing FAP-targeting agents in patients with various cancers. *J Nucl Med.* 2019;60:386-392.
42. Shi Y, Qi YF, Lan GY, et al. Three-dimensional MR elastography depicts liver inflammation, fibrosis, and portal hypertension in chronic hepatitis B or C. *Radiology.* 2021;301:154-162.
43. Yokoo T, Serai SD, Pirasteh A, et al. Linearity, bias, and precision of hepatic proton density fat fraction measurements by using MR imaging: a meta-analysis. *Radiology.* 2018;286:486-498.
44. Wood JC, Enriquez C, Ghugre N, et al. MRI R2 and R2\* mapping accurately estimates hepatic iron concentration in transfusion-dependent thalassemia and sickle cell disease patients. *Blood.* 2005;106:1460-1465.



**45.** Johansson L, Mattsson S, Nosslin B, Leide-Svegborn S. Effective dose from radiopharmaceuticals. *Eur J Nucl Med.* 1992;19:933-938.

**46.** Yin M, Glaser KJ, Manduca A, et al. Distinguishing between hepatic inflammation and fibrosis with MR elastography. *Radiology.* 2017;284:694-705.

## Tables

*Table 1.* Summary of liver FAPI uptake on PET and histologic analysis of liver tissue core biopsy and wedge sections in all subjects at baseline and at endpoint.

\* = CPA was not calculated at baseline as only core biopsies were obtained.

CPA = collagen proportionate area; FAPI = fibroblast activation protein inhibitor; PET = positron emission tomography; SUV = standardized uptake value.

<b>Animal #</b>	<b>Liver tissue</b>	<b>FAPI uptake (SUV)</b>	<b>METAVIR score</b>	<b>CPA* (%)</b>
1	Baseline core (left lobe)	1.8	F0/F1	-
	Baseline core (right lobe)	1.6	F0/F1	-
	Endpoint section 1	7.0	F4	50
	Endpoint section 2	1.5	F0/F1	15
	Endpoint section 3	5.8	F4	49
	Endpoint section 4	1.5	F0/F1	14
2	Baseline core (left lobe)	2.4	F0/F1	-
	Baseline core (right lobe)	2.0	F0/F1	-
	Endpoint section 1	2.5	F2	39
	Endpoint section 2	2.9	F2	33
	Endpoint section 3	1.7	F0/F1	9
	Endpoint section 4	1.5	F0/F1	12
3	Baseline core (left lobe)	2.2	F0/F1	-
	Baseline core (right lobe)	1.9	F0/F1	-
	Endpoint section 1	6.9	F4	40

	Endpoint section 2	2.1	F0/F1	22
	Endpoint section 3	1.8	F0/F1	13
	Endpoint section 4	4.9	F3	49
4	Baseline core (left lobe)	0.8	F0/F1	-
	Baseline core (right lobe)	1.2	F0/F1	-
	Endpoint section 1	4.7	F2	29
	Endpoint section 2	10.6	F4	77
	Endpoint section 3	4.5	F0/F1	16
	Endpoint section 4	12.6	F4	67
5	Baseline core (left lobe)	1.3	F0/F1	-
	Baseline core (right lobe)	1.3	F0/F1	-
	Endpoint section 1	8.3	F4	59
	Endpoint section 2	10.1	F4	44
	Endpoint section 3	1.6	F0/F1	13
	Endpoint section 4	1.7	F0/F1	18

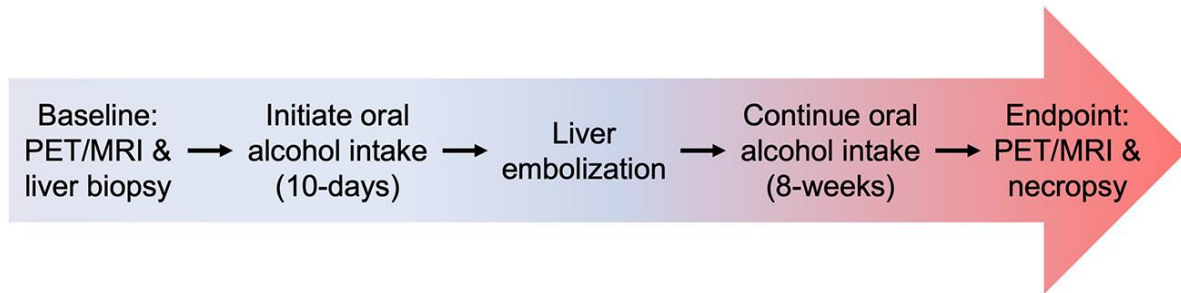


**FIGURE 1.** Study overview: after baseline PET/MRI, animals underwent a period of gradual increase in oral alcohol intake, followed by liver parenchymal transarterial embolization. After 8 weeks of oral alcohol intake, they underwent endpoint imaging followed by necropsy and tissue analysis.

MRI: Magnetic resonance imaging; PET: positron emission tomography.

Human Liver: METAVIR fibrosis score	Swine Liver: modified METAVIR fibrosis score
F0: No fibrosis	F0/F1: Expected thin bands of fibrosis seen in normal swine liver
F1: Portal fibrosis without septa	
F2: Portal fibrosis with rare septa	F2: Thickened bands of fibrosis and/or rare septa
F3: Numerous septa without cirrhosis	F3: Thickened bands of fibrosis with numerous septa without cirrhosis
F4: Cirrhosis	F4: Cirrhosis

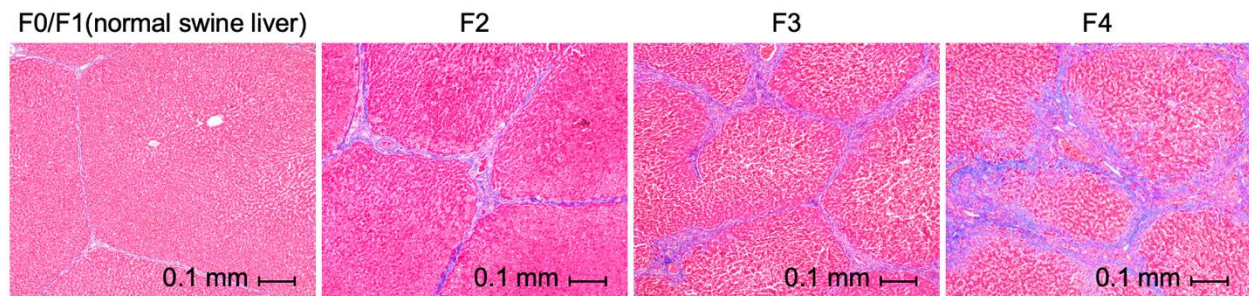


**FIGURE 2.** Modified METAVIR score to stage swine liver fibrosis: Due presence of thin bands of fibrosis in normal swine liver and absence of this finding in normal human liver, the METAVIR score used for staging human liver fibrosis was modified, such that the new stage (F0/F1) corresponds to normal swine liver with expected thin bands of fibrosis. Representative Masson's Trichrome-stained histologic slides of swine liver demonstrate the extent of fibrosis at each stage.

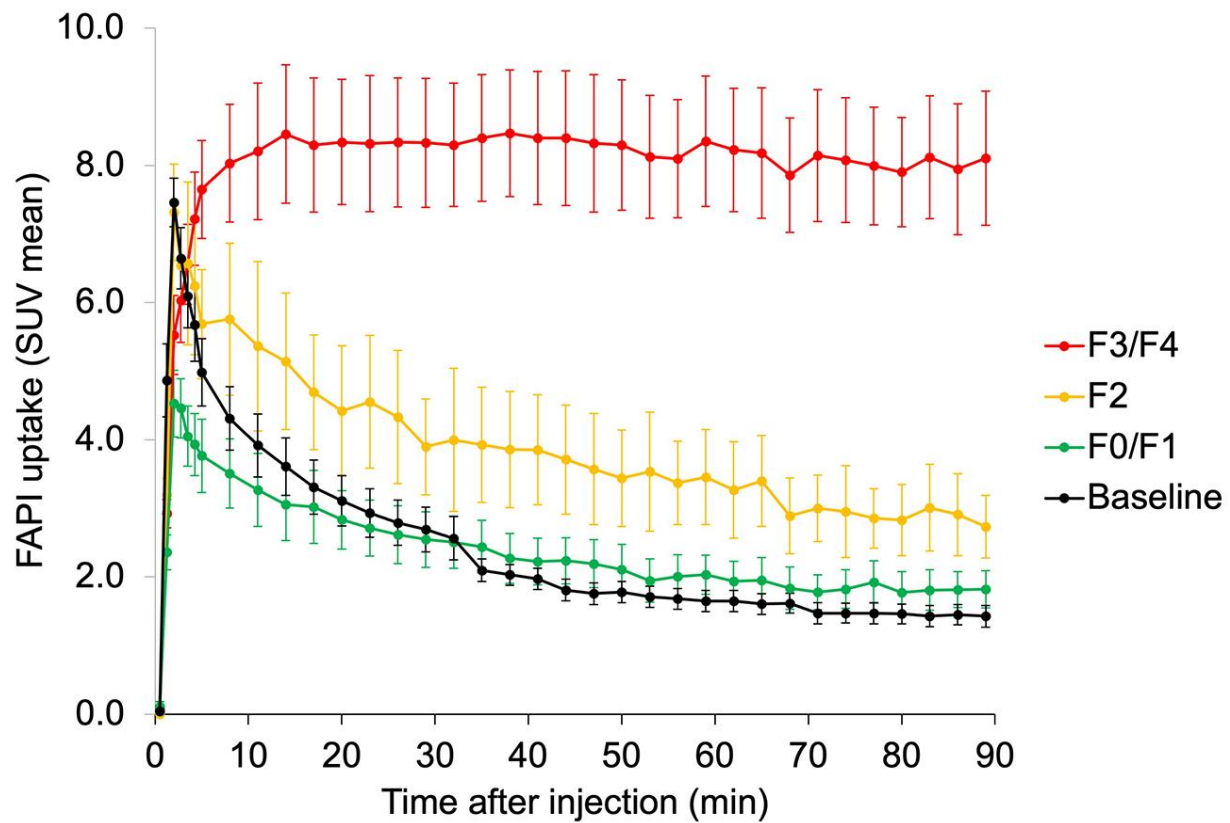


**FIGURE 3.** Pooled-data time-active curves demonstrate similar pattern of FAPI uptake by both normal liver at baseline and F0/F1 sections at endpoint (green and black curves, respectively). Conversely, there is incremental increase in delayed FAPI uptake by liver sections histologically staged as F2 and as F3/F4 ( $P < 0.001$ ).

FAPI: fibroblast activation protein inhibitor; SUV: Standardized uptake value.

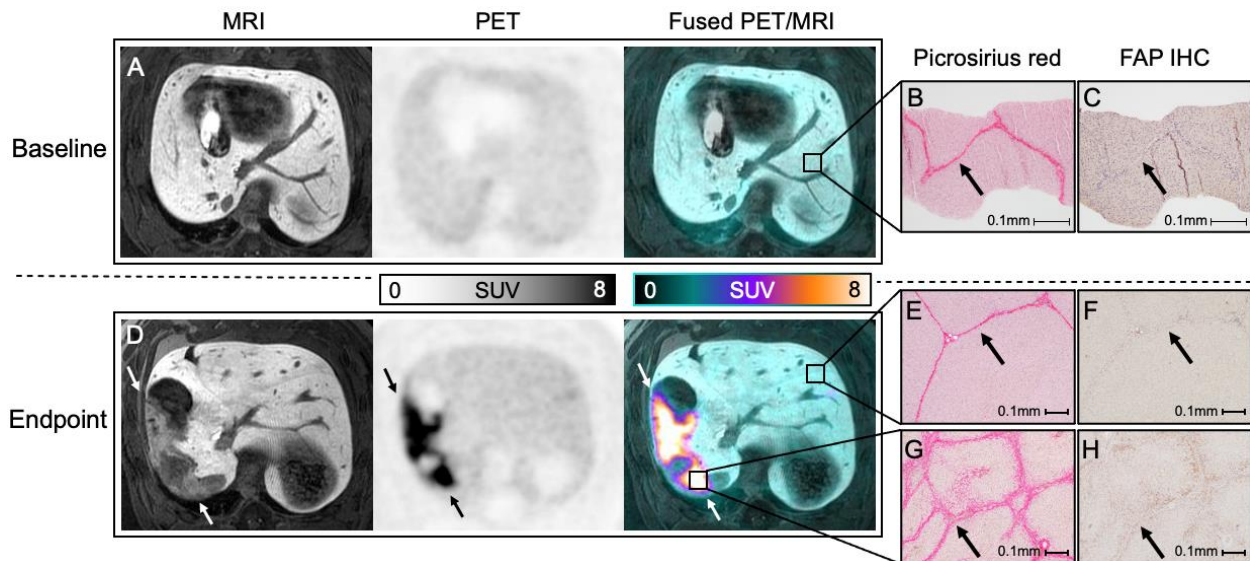


**FIGURE 4.** Imaging/histologic correlation at baseline and endpoint: (A) Baseline axial PET/MRI images of animal #5 demonstrates homogeneous liver parenchyma and mild FAPI uptake; core biopsy of the left liver lobe (at 100x magnification) demonstrates expected thin bands of fibrosis (B, arrow) with very faint staining on FAP IHC (C, arrow). (D) At endpoint, a geographical region in the right lobe demonstrates hypoenhancement on MRI and increased FAPI uptake (D, arrows). Liver sections obtained from the avid (abnormal) and non-avid (normal/spared) regions (at 40x magnification) demonstrate expected thin bands of fibrosis in normal/spared region (E, arrow) with minimal staining on FAP IHC (F, arrow), and conversely thickened bridging bands of fibrosis in the abnormal region (G, arrow), with positive staining on FAP IHC (H, arrow).

FAPI: fibroblast activation protein inhibitor; FAP IHC: fibroblast activation protein immunohistochemistry; MRI: magnetic resonance imaging; PET: positron emission tomography.

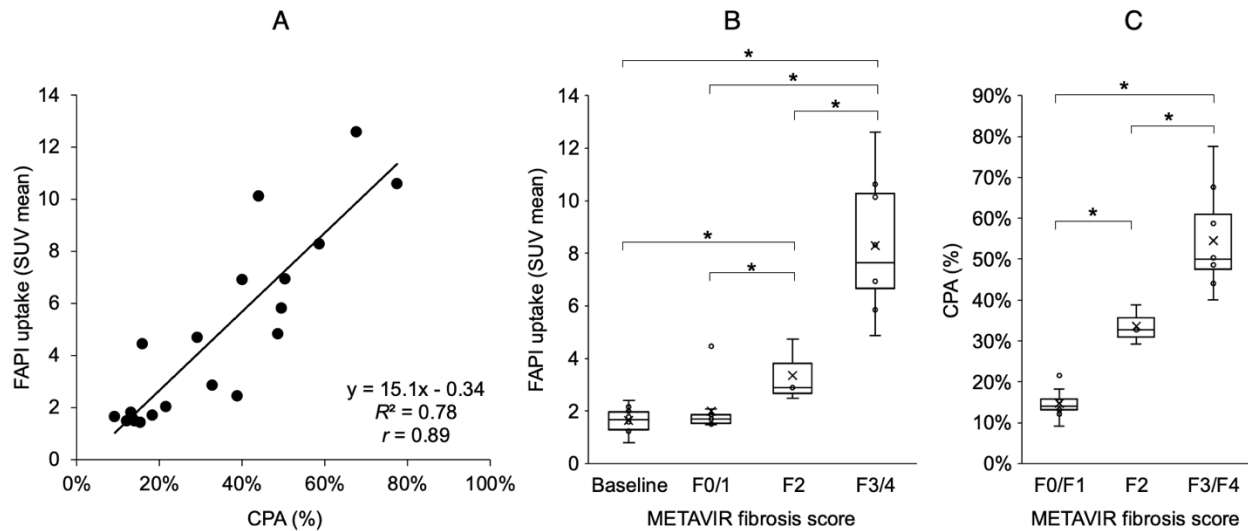


**FIGURE 5.** (A) Linear regression demonstrates a strong correlation between liver FAPI uptake and histologic CPA (Pearson correlation coefficient  $r = 0.89$ ). (B) Box-and-whisker plot of liver FAPI uptake for the METAVIR fibrosis stage groups demonstrates no significant difference between the uptake of baseline liver and endpoint liver sections staged as F0/F1 ( $P=0.338$ ); however, there is significant and incrementally higher FAPI uptake across F2 and F3/F4 stages, with minimal overlap between different stages ( $P<0.001$ ). (C) Box-and-whisker plot of histologic CPA for each METAVIR fibrosis stage group at endpoint, demonstrating significant and incrementally increased CPA with increasing fibrosis stage ( $P<0.001$ ). CPA was not performed for baseline tissues due to the relatively small amount of tissue procured through core needle biopsy at baseline.

\* = statistical significance. CPA: collagen proportionate area; FAPI: fibroblast activation protein inhibitor; SUV: standardized uptake value.



## SUPPLEMENTAL DATA

*Animal Model Preparation.* Five human-sized, age-matched, male, healthy Wisconsin Miniature Swine<sup>TM</sup> were included average age (range) of 15.3 (14-17) months and average (range) baseline weight 63 kg (56 – 76). No other inclusion or exclusion criteria were applied. No control cohort was enrolled as each animal served as its own control by the virtue of undergoing imaging and tissue sampling both at baseline and at endpoint (post fibrosis induction). No randomization was performed. Sample size was decided based on previously published literature on evaluation of liver fibrosis in swine.(46)

Animals underwent PET/MRI imaging followed by same-day ultrasound-guided core-needle liver biopsy to establish baseline histologic and imaging characteristics of the liver. A few days after baseline imaging/biopsy (to allow for recovery), gradually increasing volumes of ethanol were added to the animals' daily diets, starting from 40 mL of ethanol on day 1 to 280 mL on day 7, which was maintained as part of the diet until the study endpoint. To increase animal compliance with oral ethanol intake, ethanol was mixed with a sweetened electrolyte solution to a total volume of 2800 mL.

*Liver Embolization.* At 8 – 9 days after initiation of oral ethanol intake, animals underwent image-guided transarterial liver embolization as follows: under general anesthesia, through a percutaneous femoral arterial access, the common hepatic artery was catheterized under real-time fluoroscopic guidance. The gastroduodenal artery was coil-embolized to prevent non-target embolization and stomach/bowel necrosis. A microcatheter was advanced and positioned at the proximal proper hepatic artery, through which 30 mL of an emulsion of 1:3 (by volume) ethanol:ethiodized oil (Lipiodol, Guerbet, France) was gradually administered. The volume of embolic emulsion was based on the maximum tolerated dose demonstrated on previous

studies.(26) Catheter position was monitored and maintained by real-time fluoroscopy. Following liver embolization, animals continued oral alcohol intake for a total of 8 weeks as aforementioned, after which they underwent endpoint PET/MRI followed by necropsy and harvesting of the liver for histologic analysis.

*Radiotracer (FAPI) Production.* To a solution of 50 µg of FAPI-46 precursor (SOFIE, Dulles, VA, USA) in 100 µL ultra-trace water were added 0.35 mL of 0.07 M sodium ascorbate and 0.45 mL of 1.5 M sodium acetate in ultra-trace water. The mixture was transferred into a 10 mL sealed reaction vial. The  $^{68}\text{Ge}/^{68}\text{Ga}$  generator (GalliaPharm, Eckert & Ziegler, Radiopharma, Berlin, Germany) was eluted with 5 mL of 0.1 N HCl using a syringe pump at the rate of 2 mL/min. The eluate was passed through a sterile filter and a silicon-coated low-metal-releasing needle into the reaction vial. The reaction vial was heated by a heating block at 97° C for 20 min. After cooling for 5 min, 1 mL of 1.5 M sodium acetate was added. The crude product was sterile filtrated with a 0.22 µm Millipore filter into a final product vial. Product radiochemical purity was > 95%.

*Image Acquisition.* Radiotracer production is detailed in the Supplemental Data section. Images were acquired under general anesthesia in the supine position on a simultaneous whole-body PET/MRI scanner (Signa PET/MR, GE Healthcare, Chicago, IL, USA), using a 16-channel anterior array torso coil and a 14-channel posterior coil embedded at the isocenter of the scanner. Continuous dynamic PET data with the field of view centered over the liver were acquired for a total of 92 minutes, where FAPI was administered intravenously 1 minute after the initiation of data acquisitions. Average (range) administered radiotracer activity was 4.3 (3.5 – 4.6) MBq/kg body weight. Simultaneous MRI images were obtained during this period, including two-point Dixon images for fat-water separation for MRI-based attenuation correction, T1-weighted fat-

saturated images before and after intravenous administration of contrast (0.05 mmol/kg, gadoxetate disodium, Bayer Healthcare, NJ, USA) for anatomic localization.

*Tissue Procurement and Histologic Evaluation.* Baseline percutaneous liver core biopsies were performed under general anesthesia and real-time ultrasound guidance by a fellowship-trained abdominal radiologist or a fellowship-trained interventional radiologist. Core samples were obtained from each liver lobe, fixed in 10% formalin for 24-48 hours, and stored in 70% ethanol thereafter until embedded in paraffin. After endpoint imaging, animals were euthanized, and livers were harvested. Liver lobe surfaces were marked with ink to preserve the landmarks needed for imaging-histology co-localization and correlation. Harvested livers were sectioned using a “bread-loafing” technique in the axial (transverse) plane to resemble the axial slices on PET/MRI as accurately as possible. Liver slices were also first fixed in 10% formalin for 24-48 hours, and then stored in 70% ethanol thereafter. Using anatomic landmarks, liver areas corresponding to the ROIs on post-fibrosis images were identified, and wedge sections of the identified regions were cut out and embedded in paraffin.

Baseline and endpoint embedded tissues were processed with Masson’s Trichrome and Picrosirius red stains. Automated immunohistochemistry was performed on the Ventana Discovery Ultra BioMarker Platform (Ventana Medical Systems). Deparaffinization was carried out on the instrument, as was heat-induced epitope retrieval with cell conditioner 1 buffer (Ventana #950-224), an EDTA based buffer pH 8.4, for 48 minutes at 95 °C. The primary antibody was the anti-FAP monoclonal antibody (SP325, ab240989, Abcam, plc) diluted 1:100 in Renaissance Background Reducer Diluent (BioCare Medical #PD905) and incubated for 40 minutes at 37 °C. Slices were rinsed with reaction buffer (Ventana #950-300), incubated with Discovery OmniMap anti-rabbit horseradish peroxidase (Ventana #760-4311) for 16 minutes at 37 °C, and then rinsed

with reaction buffer. Discovery ChromoMap DAB detection kit (Ventana #760-159) was used for visualization. For negative control, slides were incubated with reaction buffer (Ventana #950-300) without primary antibody (results not shown). Slides were removed from the instrument, counterstained with Harris hematoxylin (1:5) for 45 seconds, rinsed with dH<sub>2</sub>O, dehydrated by oven drying and dipping in xylene.

Histologic review and analysis were carried out by a board-certified, fellowship-trained hepatobiliary pathologist who was blinded to all imaging results and the timepoints of tissue procurement (i.e., baseline versus endpoint). Two histologic standards were used as reference: the METAVIR fibrosis score and collagen proportionate area (CPA). The METAVIR score is an ordinal five-point scale (F0 to F4) used for human liver fibrosis staging. This scale was slightly modified for the purposes of this swine study (Figure 2). In humans, F0 is absence of fibrosis and F4 is end-stage fibrosis/cirrhosis. However, given that normal swine liver has thin, organized bands of fibrosis at baseline, F0 and F1 were grouped into one category that was assigned to normal swine liver with expected uniform thin bands of fibrosis, herein F0/F1. F2 was assigned to presence of slightly thickened bands of fibrosis and/or rare septa, F3 to thickened bands of fibrosis with numerous septa without cirrhosis, and F4 to cirrhosis.

The second utilized histologic measure of liver fibrosis, CPA, is measured as the proportion of collagen deposition area relative to the total tissue area (reported in %) on Picrosirius red-stained slides. CPA is validated as a predictor of outcomes in patients with various chronic liver diseases and can sub-classify cirrhosis and predict decompensation. (29-35) Picrosirius red-stained slides were scanned at the 20× magnification of using the Vectra Multispectral Imaging System (PerkinElmer, Inc. Hopkinton, MA, USA). Images were analyzed using the InForm software

(version 2.4, PerkinElmer, Inc. Hopkinton, MA, USA) to quantify the Picrosirius red staining in five regions within each liver section. Each region's CPA was calculated as following:

$$\text{Region's CPA} = \text{region's stained area} \div \text{region's total tissue area} \times 100\%$$

The CPA measurements at the five regions in each section were averaged to yield a per-section CPA. CPA analysis was performed only for endpoint wedge sections and not for baseline tissues due to the relatively small amount of tissue procured through core needle biopsy at baseline.

*Statistical Analysis.* Liver FAPI uptake time-activity curves were generated by plotting the pooled ROI SUVs against time for different stages of fibrosis. Box-and-whisker plots were generated to compare liver FAPI uptake and CPA across different histologic stages of liver fibrosis, using Kruskal-Wallis rank sum test. Linear regression was used to correlate liver FAPI with CPA, using the Pearson correlation coefficient. To account for the correlation among repeated measurements and their non-monotone change over time, a linear mixed effects model was used with pig- and ROI-specific random effects and piecewise linear time trend.  $P < 0.05$  was considered statistically significant. A post-hoc power analysis for testing F2 versus F0/F1, and F3/F4 versus F0/F1 stages under the current sample size was performed. All analyses were performed using R Statistical Software (Version 4.02; Foundation for Statistical Computing, Vienna, Austria).